Journal of Zhejiang University-SCIENCE A (Applied Physics & Engineering) 2024 25(4):311-323
www.jzus.zju.edu.cn; www.springer.com/journal/11582
E-mail: jzus_a@zju.edu.cn

Research Article
https://doi.org/10.1631/jzus.A2200609

Prediction of undeformed chip thickness distribution and surface roughness in ultrasonic vibration grinding of inner hole of bearings

Yanqin LI, Daohui XIANG, Guofu GAO, Feng JIAO, Bo ZHAO✉

School of Mechanical and Power Engineering, Henan Polytechnic University, Jiaozuo 454000, China

Abstract: Ultrasonic vibration grinding differs from traditional grinding in terms of its material removal mechanism. The randomness of grain–workpiece interaction in ultrasonic vibration grinding can produce variable chips and impact the surface roughness of workpiece. However, previous studies used iterative method to calculate the unformed chip thickness (UCT), which has low computational efficiency. In this study, a symbolic difference method is proposed to calculate the UCT. The UCT distributions are obtained to describe the stochastic interaction characteristics of ultrasonic grinding process. Meanwhile, the UCT distribution characteristics under different machining parameters are analyzed. Then, a surface roughness prediction model is established based on the UCT distribution. Finally, the correctness of the model is verified by experiments. This study provides a quick and accurate method for predicting surface roughness in longitudinal ultrasonic vibration grinding.

Key words: Ultrasonic vibration grinding; Undeformed chip thickness (UCT); Distribution characteristics; Surface roughness

1 Introduction

Ultrasonic vibration grinding is a non-traditional machining method that applies ultrasonic waves to the machining process (Chen FJ et al., 2010; Chen HF et al., 2013). Longitudinal ultrasonic vibration-assisted grinding has the advantages of improving machining quality and reducing surface roughness (Yang et al., 2020; Ding et al., 2022). In the ultrasonic vibration grinding process, grains cut the workpiece surface and produce numerous undeformed chips. The stochastic properties of grain location and protrusion height determine the undeformed chip thickness (UCT). It is useful to describe UCT quantitatively to obtain a deeper understanding of the ultrasonic vibration grinding process.

Grinding is a complex process with many random factors. Many assumptions have been applied to calculate the UCT to reduce the complexity. Hecker and Liang (2003) assumed that the UCT distribution followed a Rayleigh distribution and the surface groove profile was a triangle, and derived the workpiece surface roughness (R_a) prediction model using UCT. Agarwal and Venkateswara Rao (2005, 2010) established several analytical models of surface roughness assuming that the groove profile was semicircle or paraboloid. A new model considering the influence of overlap demonstrated higher precision (Agarwal and Venkateswara Rao, 2013). Malkin and Guo (2008) proposed a maximum UCT formula and introduced the height difference between adjacent abrasive particles (δ_n) to consider the static height difference between adjacent grains. Subsequently, Ding et al. (2017) proposed an improved equation that considered the effect of kinematics. They studied the UCT distribution of a textured cubic boron nitride (CBN) wheel, ignoring the randomness of grains. Setti et al. (2020) believed that the UCT was closely related to the grain protrusion height and evaluated the performance of UCT during micro-grinding. He et al. (2017) compared surface roughness values with and without the overlap effect in ultrasonic grinding. The theoretical values with the overlap effect were closer to the experimental results.

Studies of surface topography were conducted mainly by numerical simulation and usually based on the kinematic analysis method (Wang et al., 2017, 2020). In this method, the workpiece surface topography

✉ Bo ZHAO, zhaob@hpu.edu.cn
Bo ZHAO, https://orcid.org/0000-0003-0096-9324
Yanqin LI, https://orcid.org/0000-0002-4335-834X

Received Dec. 21, 2022; Revision accepted June 13, 2023; Crosschecked Dec. 21, 2023; Online first Feb. 8, 2024

is predicted by solving the minimum value of the intersection trajectory. Assume that the grain height obeyed a Gaussian distribution, Zhou and Xi (2002) established a workpiece topography prediction model by searching for the intersection of motion trajectories from high to low. Gong et al. (2002) generated a grinding wheel model with the random number generated by computer and simulated with Visual C++ to realize the prediction of R_a. Chen et al. (2018) proposed a workpiece topography generation algorithm considering the plowing effect in ultrasonic grinding. Zhou et al. (2018, 2019) proposed a new workpiece topography model considering the Poisson effect of large load in ultrasonic vibration grinding. Zhang et al. (2020) reported the combined influence of processing and ultrasonic parameters on the surface micro structure.

Although many scholars have conducted extensive studies on establishing workpiece topography models, they have rarely referred to the calculation of UCT. Darafon et al. (2013) divided the workpiece into line segments at the same time interval to calculate the UCT. This method is extremely inefficient, and lacks analysis of the distribution characteristics of UCT. Zhang et al. (2018) proposed a Newton iterative algorithm to obtain a numerical solution of the contact time t, obtained the height value of each topological point, and then calculated the UCT to obtain the UCT distribution, but the iterative algorithm is also time-consuming. Zhang et al. (2022) used an isometric method to solve the UCT of a single grain in the contact region of ultrasonic grinding and analyzed the effect of machining parameters. However, they focused mainly on radial and tangential ultrasonic grinding. To the best of our knowledge, no studies have considered the stochastic behavior of UCT in longitudinal ultrasonic vibration grinding.

In this paper, a symbolic difference method is introduced to obtain the contact position between the grain and the workpiece. The UCTs and interference widths are calculated during the longitudinal ultrasonic vibration grinding process. Then, the UCT distribution characteristics under different machining parameters are analyzed. The relationship between the UCT distribution mean value and surface roughness is obtained. Finally, the correctness of the prediction results is verified by ultrasonic grinding experiments. This study provides a quick and accurate method for predicting surface roughness in longitudinal ultrasonic vibration grinding.

2 Grain-workpiece interaction mechanism

2.1 Kinematic modeling

Fig. 1a shows a kinematic diagram of the longitudinal ultrasonic internal grinding inner hole of bearings. The grinding wheel rotates at a speed of n_s and the workpiece rotates at a speed of n_w in the opposite direction. R_w is the radius of bearing ring and R_s is the wheel radius. The motion is simplified as surface grinding in Fig. 1b. In the xO_wy coordinate system, the origin O_w is set at the highest position on the left side of the workpiece. The x-axis is in the same direction as the feed of the wheel; the y-axis is in the same direction as the workpiece's height; the z-axis is perpendicular to the xO_wy plane; b_w and l_w are the width and length

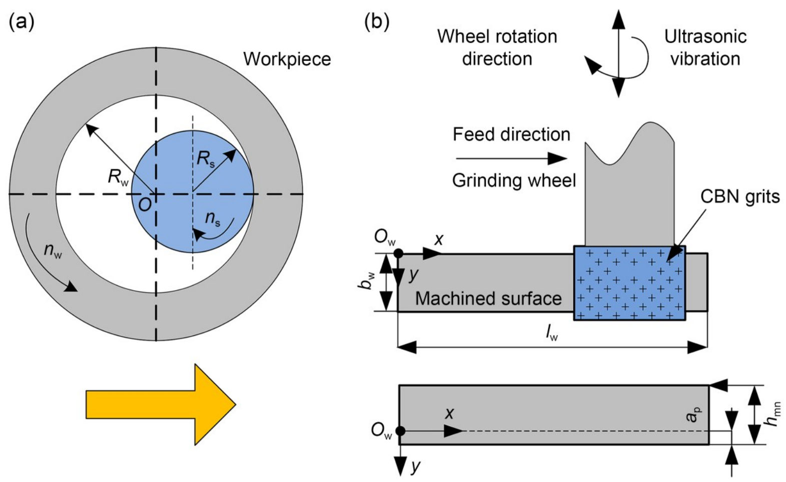

Fig. 1 Establishment of the coordinate system: (a) bearing grinding diagram; (b) motion expansion diagram

of the workpiece, respectively. The movement track equation of the grit G_{mn} at moment t is

$$\begin{cases} x_{mn}^t = x_0 + v_w t + v_w \dfrac{m\Delta d}{\omega} + (h_{mn} + R_s)\sin\theta, \\ y_{mn}^t = y_0 + n\Delta l + A\sin(2\pi ft + \varphi), \\ z_{mn}^t = z_0 + (h_{mn} + R_s)(1-\cos\theta) + h_{max} - h_{mn} - a_p, \end{cases} \tag{1}$$

where (x_0, y_0, z_0) is the coordinate of the initial contact point between grinding wheel and workpiece; Δd and Δl are the distances between the grain and the origin in the circumferential and longitudinal directions, respectively; v_w is the workpiece velocity; the index of G_{mn} is expressed as (m, n); h_{mn} is the height of G_{mn}; h_{max} is the maximum grain protrusion height; ω is the angular velocity of the grinding wheel; θ is the angular displacement expressed as $\theta=\omega t-m\Delta d/R_s$; A is the ultrasonic amplitude; f is the ultrasonic frequency; a_p is the grinding depth. The phase difference between different grinding grains is given by $\varphi=2\pi f\Delta d/(R_s\omega)$. Because the grinding arc length is much less than the grinding wheel diameter, the simplified formulas $\sin\theta\approx\theta$, $\cos\theta\approx\theta^2/2$ from Zhou et al. (2019) are used in the calculation process. Therefore, the velocity of G_{mn} at moment t is as follows:

$$\begin{cases} v_x^{mn} = v_w + (h_{mn} + R_s)\,\omega\left(1 - \dfrac{\theta^2}{2}\right), \\ v_y^{mn} = 2\pi fA\cos(2\pi ft + \varphi), \\ v_z^{mn} = \omega\theta(h_{mn} + R_s). \end{cases} \tag{2}$$

2.2 Grain-workpiece interaction in the ultrasonic grinding process

The movement track of grit G_{mn} is shown in Fig. 2a, and the workpiece in Fig. 2b. The workpiece is discretized by Δx as a series of sampling planes in the x direction, and the sampling plane is discretized by Δy as a series of vertical line segments. The calculation precision is determined by the sampling spacing. In Fig. 2c, the length of each line segment represents the height of the workpiece. The initial value for all grid points in the height direction is set as z_0. Thus, the coordinate of the grid point (x_{ij}, y_{ij}, z_{ij}) is expressed as

$$\begin{cases} x_{ij} = i\Delta x, \\ y_{ij} = j\Delta y, \\ z_{ij} = z_0, \end{cases} \tag{3}$$

where j represents the number of the vertical line segment within the sampling plane i.

In the ultrasonic grinding contact zone, numerous grains cut the workpiece surface to achieve material removal. All cutting grains will produce chips, and the interference depths are equal to the UCTs. When the grains slide or plow across the workpiece surface, the interference depths should also be regarded as the UCTs. Therefore, the UCT can be determined by solving the interference depth.

In this study, a symbolic difference method is proposed to obtain the initial contact position of the grain and the workpiece, which significantly improves the calculation efficiency. The difference between the coordinates of the grain and the grid point is regarded as the function $f(x_c)$ (x_c is the x coordinate of the contact position), namely $f(x_c)=x_c-x_{ij}$. Suppose there is x_c to make $f(x_c)=0$, i.e., $x_c=x_{ij}$. The prerequisite for the existence of the solution of the function is that $f(x_c)$ is a monotone function in the interval (x_1, x_2), and $f(x_1)f(x_2)<0$, i.e., $f(x_1)$ and $f(x_2)$ have different signs. Therefore, searching for the position of the contact point can be understood as the position of the function sign transformation. The steps of the symbolic difference method are as follows, and an example is shown in Table 1.

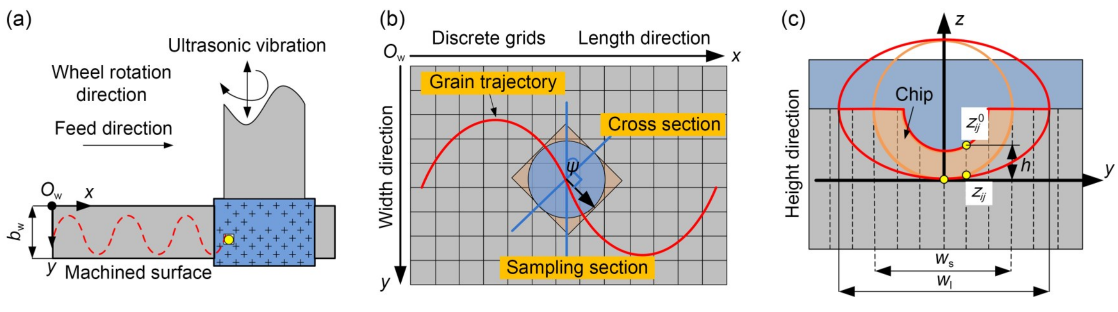

Fig. 2 Chip generation mechanism illustration: (a) ultrasonic grinding diagram; (b) workpiece grids; (c) UCT and width

Table 1 Example of the symbolic difference method

$f(x_c)$	sign($f(x_c)$)	diff($f(x_c)$)	sign(diff($f(x_c)$))	abs(sign(diff($f(x_c)$)))
−3	−1			
−2	−1	0	0	0
−1	−1	0	0	0
1	1	2	1	1
2	1	0	0	0
3	1	0	0	0
−1	−1	−2	−1	1

(1) The 'sign' function is used to solve $f(x_c)$. If $f(x_c)<0$, 'sign' returns −1; if $f(x_c)>0$, 'sign' returns 1.

(2) The difference function 'diff' is adopted to search the position of sign transformation. If diff($f(x_c)$)<0, it means the function decreases and is denoted as 'sign(diff($f(x_c)$))=−1'; if diff($f(x_c)$)>0, it means the function increases and is denoted as 'sign(diff($f(x_c)$))=1'. Both cases indicate sign transformation.

(3) Searching for the contact point. Both the maximum and minimum values meet the conditions, so the 'abs' function is used to determine the position of the contact point, i.e., x_c.

(4) The coordinate values y_c and z_c are obtained according to the trajectory Eq. (1). Thus, the position of the grain can be determined.

During the longitudinal ultrasonic grinding process, the movement path of a grain on the xO_wy plane is similar to a sinusoidal curve and the cross section of the grain movement path is perpendicular to the velocity direction (Fig. 2b). The angle ψ between the sampling section and the cross section can be expressed as

$$\psi=\arctan\left(-\frac{v_x^{\mathrm{mn}}}{v_y^{\mathrm{mn}}}\right)=\arctan\left[-\frac{v_{\mathrm{w}}+(h_{\mathrm{mn}}+R_{\mathrm{s}})\omega\left(1-\dfrac{\theta^2}{2}\right)}{2\pi fA\sin\left(2\pi ft+2\pi f\dfrac{\Delta d}{R_{\mathrm{s}}\omega}\right)}\right]. \tag{4}$$

In the sampling section, the contour of the grinding groove is an ellipse (Fig. 2c). The long axis of the ellipse is w_l and the short axis is w_s. The groove contour can be expressed as

$$\frac{(z-z_c)^2}{(w_l/2)^2}+\frac{(y-y_c)^2}{(w_s/2)^2}=1. \tag{5}$$

Therefore, w_l is

$$w_l=\frac{d_g}{\sin\psi}=\frac{d_g}{\sin\left[\arctan\left|-\dfrac{v_{\mathrm{w}}+(h_{\mathrm{mn}}+R_{\mathrm{s}})\omega\left(1-\dfrac{\theta^2}{2}\right)}{2\pi fA\sin\left(2\pi ft+2\pi f\dfrac{\Delta d}{R_{\mathrm{s}}\omega}\right)}\right|\right]}, \tag{6}$$

where d_g is the diameter of the grain.

When the value of w_l is determined, the cutting groove contour Eq. (5) is determined accordingly. Fig. 2c shows that the groove width generated by ultrasonic grinding is wider than that of traditional grinding.

(5) Eq. (3) is substituted into the contour Eq. (5) of grain to solve w_s and w_l.

Whether the grain and workpiece intersect can be determined from the interference depth and width values. Supposing that the equation is not solvable, there is no intersection between the grain and the vertical line. Instead, we can solve the equation and obtain $z=z_{ij}$ and $y=y_{ij}$. This value is compared with the initial height value z_0. If $z_{ij}<z_0$, the grain intersects the vertical line (Fig. 2c). Assume that the interfered workpiece material is completely removed, the interference depth is $h=z_0-z_{ij}$, and the interference width is $w=2w_l$. h and w are stored in the arrays $\boldsymbol{H}$ and $\boldsymbol{W}$, counted as u and v, respectively. Meanwhile, considering the trajectory interference effect of grains, z_0 is replaced by z_{ij}. Thus, the UCT mean value in the sampling plane i is expressed as

$$h_{\mathrm{mean}}^i=\frac{1}{u}\sum_0^u h_u. \tag{7}$$

For sampling sections at different locations, the values of w_l are different, meaning that there should be different groove contour equations, and the degree of groove widened is dynamic. Thus, the average interference width in the sampling plane i is expressed as

$$w_{\mathrm{mean}}^i=\frac{1}{v}\sum_0^v w_v. \tag{8}$$

(6) When all sampling planes are calculated, the trajectory of a single grain cutting the workpiece surface is completed. When all grains traverse the workpiece surface according to this method, the interference depths between all grains and the workpiece can be obtained under given processing condition. When all the

grains pass through the workpiece surface, the initial surface residual height z_{ij}^0 will be updated as Eq. (9), and the machined surface height of the workpiece can be obtained.

$$z_{ij}=\min\left\{z_{ij}, z_{ij}^0\right\}. \tag{9}$$

The grain number N on the grinding wheel surface determines the simulated workpiece surface. In the simulation process, a workpiece surface with a length of 1.5 mm was processed by 1880 grains. The flow of the surface topography and the calculation of UCT distribution algorithm are shown in Fig. 3.

In Fig. 3, n is the number of grain randomly generated; k is the calculated grain number; v_s is the velocity of the grinding wheel; $d_g \in N(\mu, \sigma^2)$ represents d_g follows the normal distribution; μ is the average value; σ is the standard deviation; $\delta_i \in U(c, d)$ represents the grain position offset δ_i follows the uniform distribution; c and d are the upper and lower bounds, respectively.

2.3 Influence rule of machining parameters on UCT distribution

2.3.1 UCT distribution characteristics

Based on the above numerical simulation method, under the conditions of grinding parameters n_s=2000 r/min, v_w=1200 mm/min, a_p=20 μm, and A=4 μm, the grain protrusion height follows a normal distribution (Fig. 4a), and the UCT distribution result is as

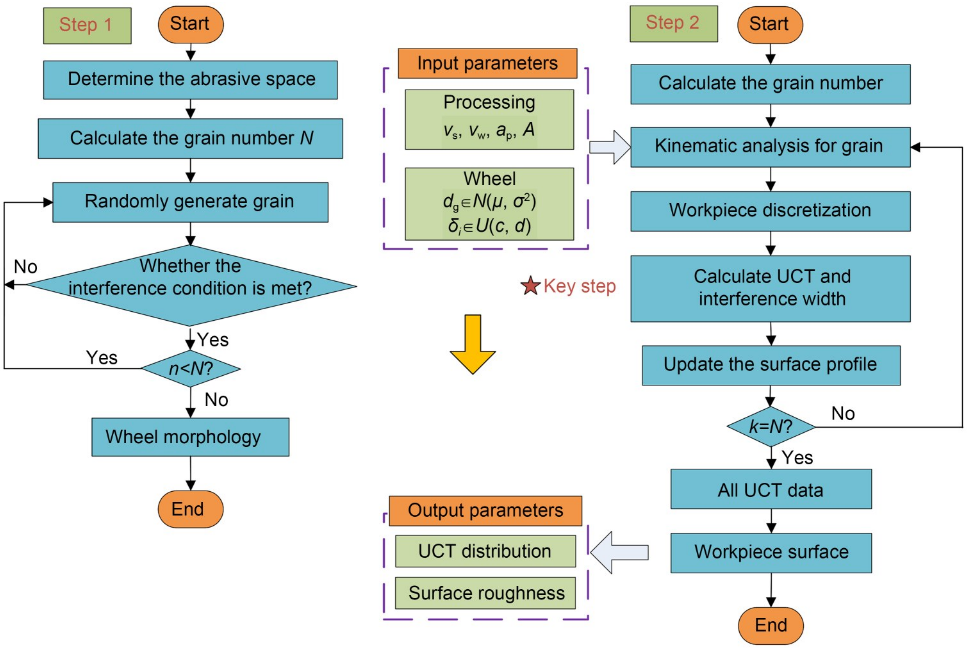

Fig. 3 Flowchart of workpiece surface topography and UCT distribution generation algorithm

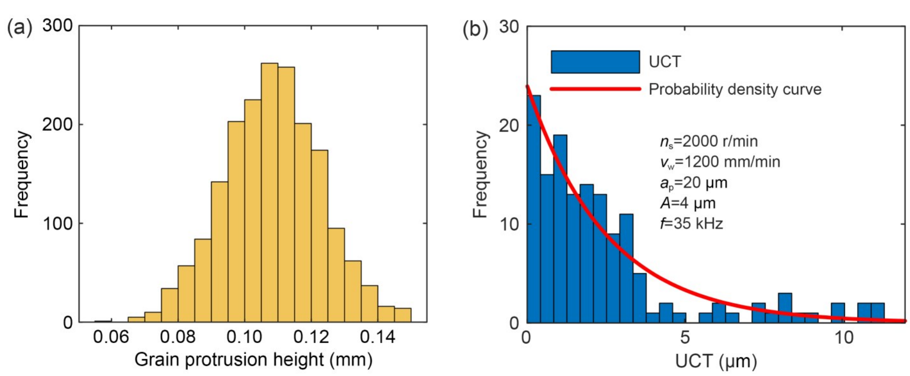

Fig. 4 Numerical simulation results: (a) grain protrusion height distribution; (b) UCT distribution

shown in Fig. 4b. The UCT distribution is represented by a probability density histogram from which the frequency variation of UCT in a specific range can be observed. The minimum cutting thickness is 0 μm, indicating that grains are not involved in the grinding. The maximum chip thickness is 13 μm.

An exponential function is used to fit the histogram, and its probability density function can be expressed as

$$P(h)=\begin{cases}\chi e^{-\chi h}, & h>0,\\ 0, & \text{else},\end{cases} \tag{10}$$

and the expected value $E(h)$ of the exponential distribution is

$$E(h)=\frac{1}{\chi}, \tag{11}$$

where χ is the rate parameter and can be calculated by the mean value of UCT.

In addition, the mean UCT value h_{mean}, the maximum chip thickness h_{max}, and the variance v_{ar} of the UCT distribution can all be used as quantitative characteristic parameters to describe the UCT distribution.

2.3.2 Influence rule of ultrasonic parameters on the UCT distribution

The motion trajectories of the grains in longitudinal ultrasonic grinding differ from those in traditional grinding, so the UCT distribution forms are also different. The UCT distribution histograms obtained under different ultrasonic amplitudes and frequencies shown in Fig. 5 are based on the grinding parameters n_s= 2000 r/min, v_w=1200 mm/min, and a_p=20 μm. These UCT distributions follow an exponential distribution. The characteristic parameters extracted from the UCT distributions under different ultrasonic amplitudes and frequencies are shown in Tables 2 and 3.

As shown in Table 2, with the increase of A, h_{max} increases from 11.8435 to 12.5179 μm; h_{mean} decreases from 2.5225 to 2.3802 μm; v_{ar} increases from 6.9264

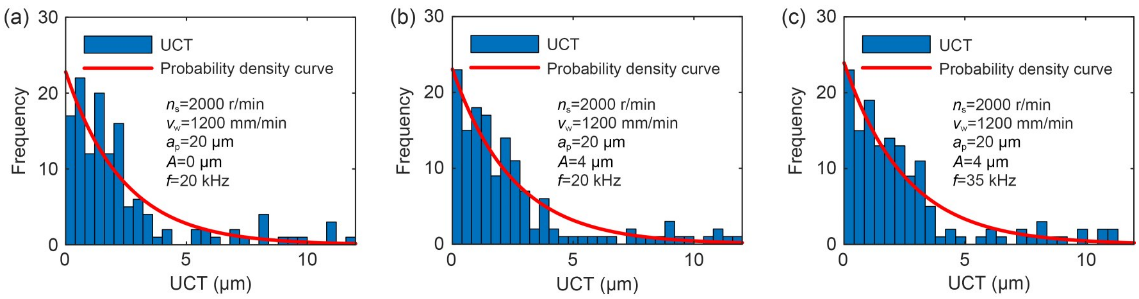

Fig. 5 UCT distribution histograms under different ultrasonic amplitudes and frequencies (a–c)

Table 2 UCT distribution parameters under different ultrasonic amplitudes

No.	A (μm)	h_{mean} (μm)	v_{ar} (μm)	h_{max} (μm)	N_e	w_{mean} (μm)	R_a (μm)
1	0	2.5225	6.9264	11.8435	136	15.1029	1.2825
2	1	2.4535	7.0024	11.9984	139	15.2428	1.2513
3	2	2.4245	7.1003	12.1474	140	15.2929	1.2125
4	3	2.3842	7.1735	12.2914	142	15.3768	1.1680
5	4	2.3802	7.2799	12.5179	142	15.5986	1.1415

N_e: number of effective grains; w_{mean}: mean interference width

Table 3 UCT distribution parameters under different ultrasonic frequencies

No.	f (kHz)	h_{mean} (μm)	v_{ar} (μm)	h_{max} (μm)	N_e	w_{mean} (μm)	R_a (μm)
1	20	2.5111	7.4701	11.8968	145	14.7241	1.3052
2	25	2.5424	7.3553	12.5011	145	15.3322	1.3164
3	30	2.5759	7.6635	12.6807	145	15.5069	1.3312
4	35	2.5410	7.3270	12.5623	145	15.7882	1.3125

to 7.2799 μm; N_e increases from 136 to 142. This is because the sinusoidal grain movement track of ultrasonic grinding is longer than the linear track of traditional grinding, causing the UCT to be more uniform and smaller. The w_{mean} between the grain and workpiece also increases gradually, indicating that the width of the grinding groove increases. This provides the basis for obtaining a better surface than traditional grinding. It can be concluded that the ultrasonic amplitude affects the UCT distribution.

As shown in Table 3, with the increase of f, the parameters such as h_{max} and h_{mean} first increase and then decrease; N_e remains unchanged; w_{mean} increases; R_a shows the same change trend as h_{mean}. According to the above analysis, longitudinal ultrasonic grinding can improve the workpiece surface quality. Because the sine trajectory of ultrasonic grinding is superimposed, the UCT mean value decreases, and the grinding grooves are widened, and the increase of A enhances the repeated interference effect, which is the fundamental reason for the reduction of surface roughness.

2.3.3 Influence rule of machining parameters on UCT distribution

Fig. 6 shows the UCT distribution histograms at different machining parameters. For all probability density histograms, they follow the exponential distribution.

Obviously, there are significant differences in UCT distribution at different machining parameters. When n_s increases, the number of grains with chip thickness between 0 and 5 μm increases (Figs. 6a and 6b). h_{max} decreases, which means that the chip thickness distribution tends to be concentrated. h_{mean} and N_e decrease. This is because with the increase of n_s, h_{max} decreases and the radial interference depth of the grinding wheel decreases, resulting in the reduction of N_e. Meanwhile, under the same v_w, when n_s increases, the workpiece feed decreases within the time interval of adjacent abrasive motion; the chip thickness of a single grain decreases; h_{mean} decreases; R_a decreases correspondingly from 1.4172 to 0.9801 μm (Table 4).

The effect of the v_w on the UCT distribution is shown in Figs. 6a and 6c. With the increase of v_w, the number of grains with chip thickness between 0 and 5 μm decreases; h_{max} increases; h_{mean} increases. v_{ar} increases, and N_e rises from 143 to 153. This is because as v_w increases, the radial interference depth increases, resulting in the rise of N_e and h_{mean}, and a corresponding increase in R_a from 1.1904 to 1.4381 μm.

The effect of a_p on the UCT distribution is shown in Figs. 6a and 6d. With the increase of a_p, h_{max} increases from 2.0248 to 16.1930 μm, indicating that the range of chip thickness distribution becomes dispersed. h_{mean} increases from 0.7535 to 3.0559 μm, and v_{ar} increases from 0.1911 to 11.9630 μm. The UCT distribution becomes more and more uneven, and R_a increases correspondingly from 0.3243 to 1.3142 μm (Table 4).

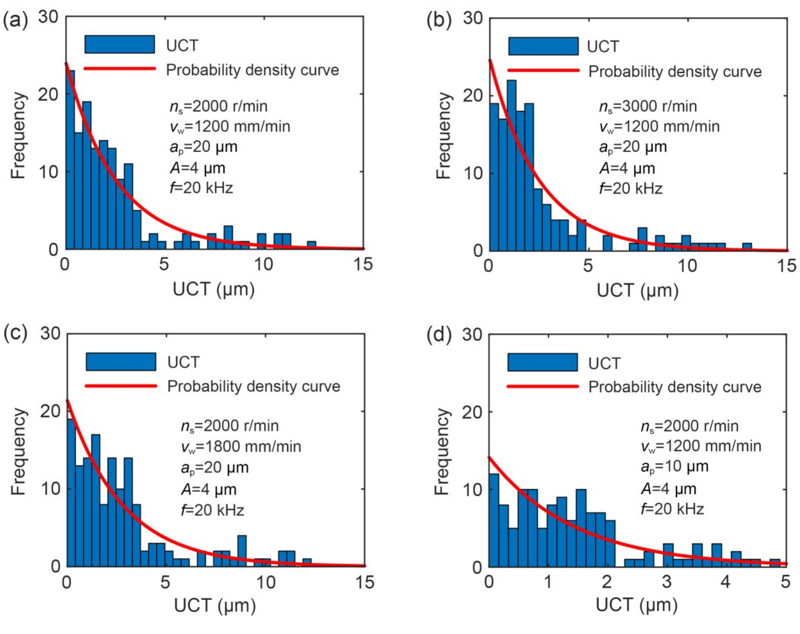

Fig. 6 UCT distribution histograms under different machining parameters (a–d)

Table 4 UCT distribution parameters under different grinding parameters

No.	n_s (r/min)	v_w (mm/s)	a_p (μm)	h_{mean} (μm)	v_{ar} (μm)	h_{max} (μm)	N_e	R_a (μm)
1	1000	20	20	3.0626	7.7726	12.7725	154	1.4172
2	1500	20	20	2.7025	7.4864	12.7868	149	1.3621
3	2000	20	20	2.5410	7.3270	12.5623	145	1.2704
4	2500	20	20	2.5249	7.4494	12.6701	145	1.0862
5	3000	20	20	2.5022	7.4223	12.5744	140	0.9801
6	2000	15	20	2.4406	7.2574	12.2590	143	1.1904
7	2000	20	20	2.5410	7.3270	12.5623	145	1.2703
8	2000	25	20	2.6820	7.4501	12.7312	147	1.2934
9	2000	30	20	2.8146	7.3491	12.1588	147	1.3512
10	2000	35	20	2.8769	7.5231	12.8036	153	1.4381
11	2000	20	5	0.7535	0.1911	2.0248	112	0.3243
12	2000	20	10	1.4408	1.3065	4.8778	125	0.6205
13	2000	20	15	2.0565	3.7403	8.7152	133	0.8842
14	2000	20	20	2.5410	7.3270	12.5623	145	1.2701
15	2000	20	25	3.0559	11.9630	16.1930	153	1.3142

2.4 Regression model of surface roughness

The mapping relationship between h_{mean} and R_a can be established from the data in Table 3, as illustrated in Eq. (12) and Fig. 7.

$$R_a = a + b \cdot h_{mean}, \tag{12}$$

where a and b are the intercept and slope of the regression line, which are −0.0519 and 0.4962, respectively. The Pearson correlation coefficient is 0.95256. In statistics, the Pearson correlation coefficient is used to evaluate the correlation between two variables. A value between 0.8 and 1.0 is regarded as indicating a strong correlation (Tao et al., 2022).

As shown in Fig. 7, R_a is proportional to h_{mean} and the data fall on the fitted line with little deviation. This means that the h_{mean} reflects the stochastic characteristics of the grains and has a direct influence on R_a. The establishment of the mapping relationship between the h_{mean} and R_a provides an effective way to predict surface roughness.

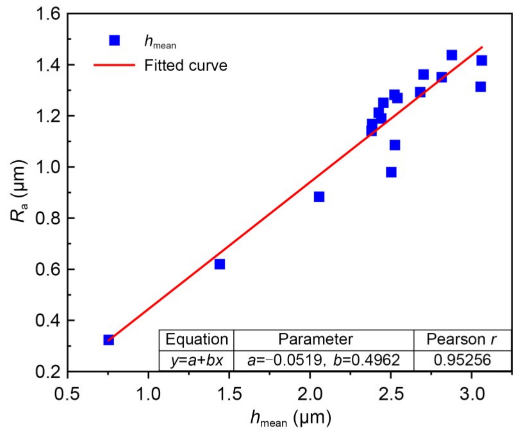

Fig. 7 Relationship between h_{mean} and R_a

3 Experimental verification

3.1 Experimental scheme

To verify the proposed surface topography model and the R_a predictive effect, a single factor experiment of ultrasonic grinding was carried out. Fig. 8 shows the experimental platform, which includes ultrasonic generator, ultrasonic tool holder, and force measuring system. The ultrasonic generator generated the current signal and transmitted it to the transducer. The transducer converted received high-frequency electrical signals into mechanical signals. The horn amplified mechanical signals to produce vibration. The ultrasonic tool holder was installed on the spindle (Fig. 8b). The amplitude was 4 μm and the frequency was 35 kHz. A dynamometer (Kistler 9257B, Kistler, Switzerland) was used to measure the grinding force.

The diameter of the ceramic bonded CBN grinding wheel was 30 mm. The workpiece was made of GCr15 bearing steel cut into rectangular blocks of 20 mm×15 mm×10 mm. The grain size was 100# and

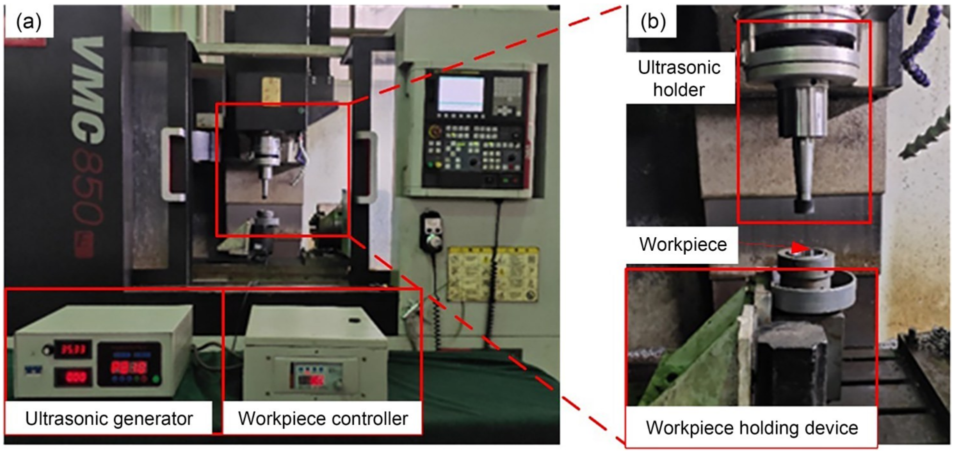

Fig. 8 Diagram of the ultrasonic grinding experimental platform (a) and platform details (b)

the grinding wheel concentration was 100%. The grinding wheel was dressed by a diamond roller. The dressing parameters were: speed ratio q=0.6, dressing speed v_{fd}=300 mm/min, and dressing depth a_d=2 μm, and the wheel was dressed three times during every experiment. Grinding parameters are listed in Table 5.

Table 5 Grinding parameters used in the experiment

Item	Description
Grinding mode	Up grinding
Lubrication method	Dry grinding
n_s (r/min)	1000, 1500, 2000, 2500, 3000
v_w (mm/s)	15, 20, 25, 30, 35
a_p (μm)	5, 10, 15, 20, 25
A (μm)	0, 1, 2, 3, 4

3.2 Experimental results

3.2.1 Surface topography

The surface topography of the workpiece is an intuitive index to judge the surface quality. Fig. 9 shows a comparison of measured and simulated morphologies under different amplitudes (n_s=2000 r/min, v_w=20 mm/s, and a_p=20 μm). Figs. 9a–9c show the workpiece surface morphologies measured by microscopy (VHX-2000C, Keyence, Japan). Figs. 9d–9f show the simulated workpiece surface morphologies.

The movement trajectory of grains was mapped to the workpiece surface, and surface quality was reflected through the characteristics of the grooves on the workpiece surface. As shown in Figs. 9a and 9d, parallel linear grooves were formed along the grinding direction in the traditional grinding process, and an obvious plastic accumulation phenomenon occurred (Fig. 9a), which affected the surface roughness of the workpiece.

The workpiece surface morphologies of ultrasonic vibration grinding under A=2 and 4 μm are shown in Figs. 9b and 9c. Compared with traditional grinding, the sinusoidal trajectory of the grains forms a wavy texture on the workpiece surface. The wavy lines in Fig. 9c become more curved. The range of motion trajectories of the grains is extended; the grooves are denser; the repetition rate of grinding grooves between axial and circumferential adjacent grinding grains is staggered, and a relatively flat surface topography can be obtained. The simulated workpiece surface morphologies present similar characteristics (Figs. 9e and 9f).

The ultrasonic grinding process can form a wavy texture due to the grain's sinusoidal trajectory. As the ultrasonic amplitude increases, the waves become more apparent. These results prove that the simulation model can obtain the morphological characteristics of ultrasonic grinding under different machining parameters.

3.2.2 Surface texture

The measured and simulated surface texture results at three typical wheel speeds (1000, 2000, and 3000 r/min) are shown in Fig. 10.

The experimental results were affected by many factors, including grain wear and the vibration of the machine tool. Therefore, the texture morphology was not perfect. The texture spacing of the machined surface can be measured by the distance between adjacent wave troughs of the texture structure.

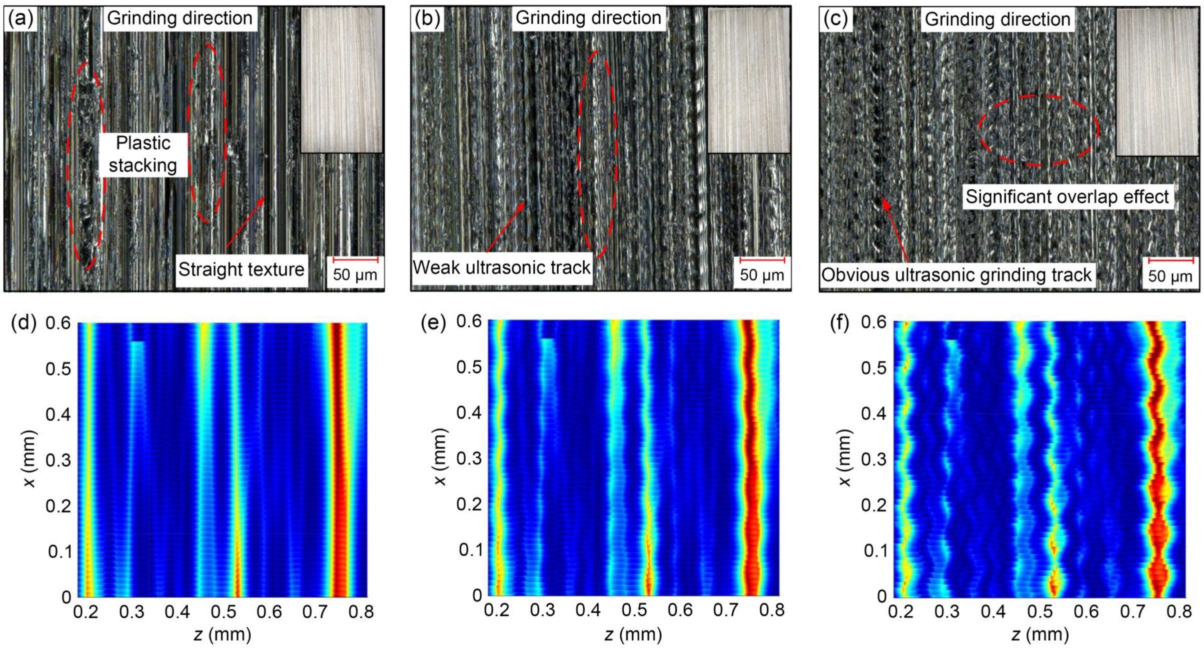

Fig. 9 Surface morphology under different ultrasonic amplitudes: (a–c) measured morphology with A=0 μm (a), A=2 μm (b), and A=4 μm (c); (d–e) simulated morphology with A=0 μm (d), A=2 μm (e), and A=4 μm (f). References to color refer to the online version of this figure

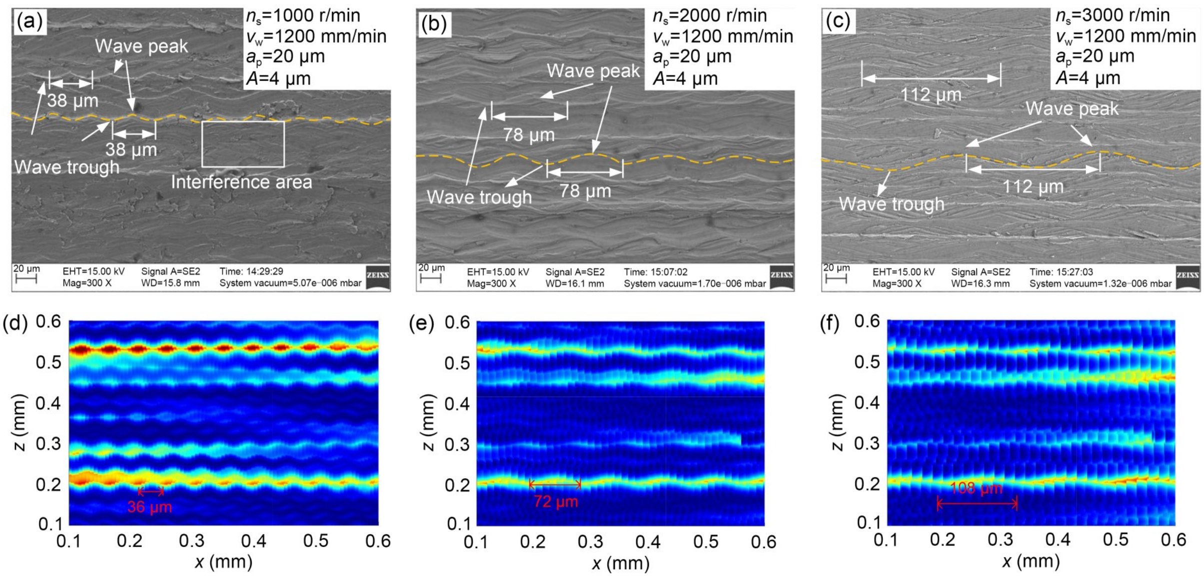

Fig. 10 Surface texture under different wheel speeds: (a–c) measured texture with n_s=1000 r/min (a), n_s=2000 r/min (b), and n_s=3000 r/min (c); (d–e) simulated texture with n_s=1000 r/min (d), n_s=2000 r/min (e), and n_s=3000 r/min (f). References to color refer to the online version of this figure

There were repeated wave-like textures on both the measured and simulated surfaces due to the ultrasonic vibration. The shape and distribution of the texture structure of simulation results were similar to those of the experimental results. Both results showed that the size of the texture structure was related to the wheel speed. On the measured surface, the texture spacing was nearly 38, 78, and 112 μm at wheel speeds of 1000, 2000, and 3000 r/min, respectively. On the simulated surface, the corresponding texture spacing was nearly 36, 72, and 108 μm, respectively. The simulated spacings closely matched the measured spacings. In addition, the number of texture structures from the experimental results was the same as that from the simulation results.

The comparison between the simulation and the experimental results shows that the proposed model can describe the shape and spacing of the texture structures in ultrasonic vibration grinding, which indicates the feasibility of our proposed model.

3.2.3 Surface roughness

The surface roughness of the workpiece under different machining parameters was measured using a surface contact profiler Time 3231 (Time, China). To reflect the surface roughness fully and reasonably, after taking five measurements perpendicular to the grinding direction at different positions, the average value was calculated as the experimental results. Fig. 11 shows the simulation and experimental results.

When n_s increases, R_a decreases (Fig. 11a). This is because when n_s increases, the mean value of the UCT distribution decreases, the overall level of chip thickness decreases, and the distribution variance decreases. The distribution becomes more uniform. Therefore, R_a decreases accordingly.

Figs. 11b and 11c show that R_a increases with the increase of v_w and a_p. The influence of v_w and a_p on the distribution characteristics of UCT is opposite to that of n_s. When v_w and a_p increase, the overall level of chip thickness increases, and h_{mean} increases correspondingly, which leads to the rise of R_a.

In addition, when A increases, R_a does not change much. It tends to decrease, which may be due to the high dressing depth, which flattens the grains and results in the insignificant ultrasonic effect (Fig. 11d). In short, the variation trend of experimental results is consistent with the simulated values. The error between the simulated roughness and the experimental roughness is 14.3% at most, which verifies the model's effectiveness. The deviation between experimental and simulation results is due to the effect of uncontrollable factors such as grain wear and spindle vibration.

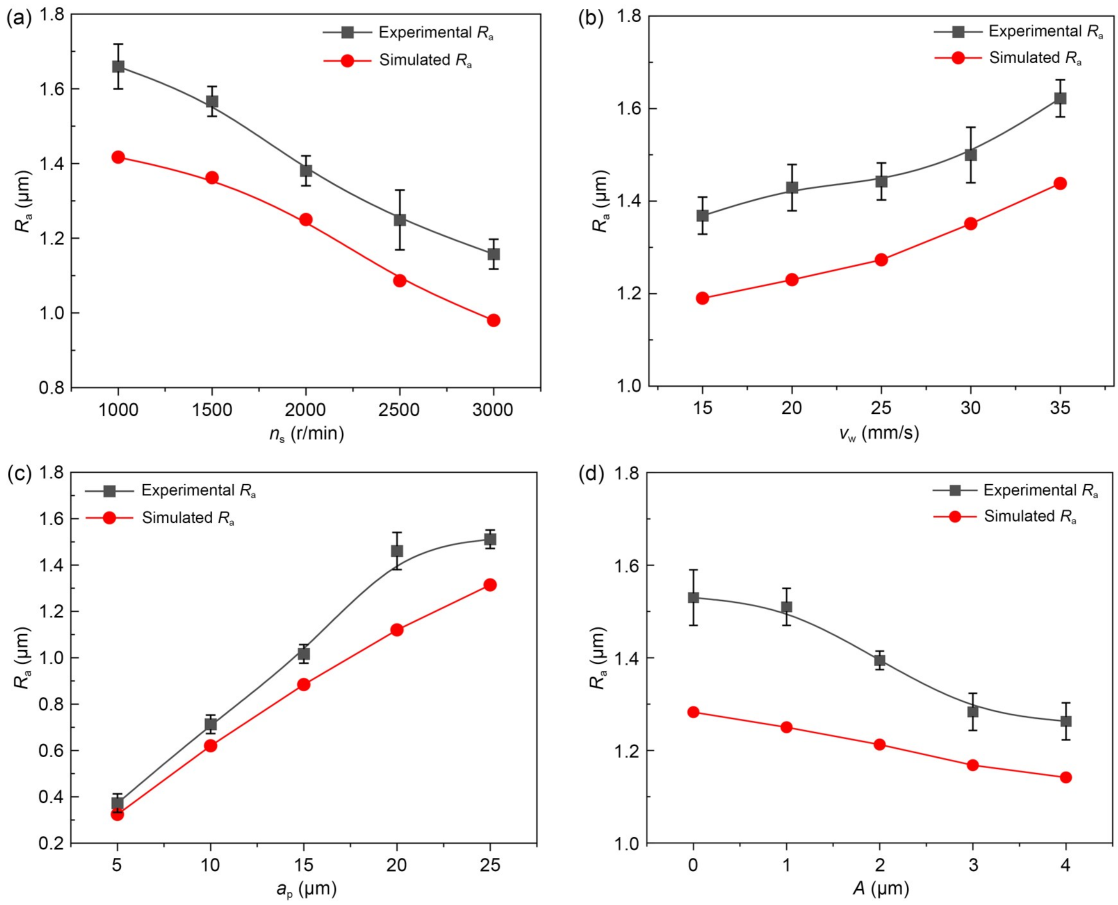

Fig. 11 Surface roughness under different grinding parameters: (a) influence of wheel speed; (b) influence of workpiece velocity; (c) influence of grinding depth; (d) influence of ultrasonic amplitude

4 Conclusions

This study provides a quick and effective method to calculate UCT and width in longitudinal ultrasonic vibration grinding, and a surface roughness prediction model related to the UCT distribution characteristics. The following conclusions can be summarized:

1. Based on the grain moving trajectory during ultrasonic vibration grinding, a symbolic difference method was proposed to calculate UCT and width to raise the simulation efficiency.

2. The UCT distribution in the ultrasonic vibration grinding process follows an exponential distribution. The characteristic parameters of UCT distribution were extracted. The application of ultrasonic waves can change UCT and width, enhance the repeated interference effect, and reduce the surface roughness.

3. The influence rules of grinding parameters on the UCT distribution characteristics were analyzed. A linear relationship is found between R_a and h_{mean}. The experimental results show the same variation tendency as the simulated values, with a maximum deviation of 14.3%.

4. High grinding wheel speed, low workpiece speed, small grinding depth, and an appropriate ultrasonic amplitude are conducive to obtaining lower UCT, forming a smoother workpiece surface.

Acknowledgments

This work is supported by the National Key Research and Development Program of China (No. 2018YFB2000402), the Open Fund Project of Xinchang Research Institute of Zhejiang University of Technology, and the Fundamental Research Funds for the Universities of Henan Province, China (No. NSFRF200102).

Author contributions

Yanqin LI investigated and wrote the original draft. Daohui XIANG processed the corresponding data. Guofu GAO helped organize the manuscript. Feng JIAO helped modify the manuscript. Bo ZHAO designed the research.

Conflict of interest

Yanqin LI, Daohui XIANG, Guofu GAO, Feng JIAO, and Bo ZHAO declare that they have no conflict of interest.

References

Agarwal S, Venkateswara Rao P, 2005. A probabilistic approach to predict surface roughness in ceramic grinding. *International Journal of Machine Tools and Manufacture*, 45(6): 609-616.
https://doi.org/10.1016/j.ijmachtools.2004.10.005

Agarwal S, Venkateswara Rao P, 2010. Modeling and prediction of surface roughness in ceramic grinding. *International Journal of Machine Tools and Manufacture*, 50(12): 1065-1076.
https://doi.org/10.1016/j.ijmachtools.2010.08.009

Agarwal S, Venkateswara Rao P, 2013. Predictive modeling of force and power based on a new analytical undeformed chip thickness model in ceramic grinding. *International Journal of Machine Tools and Manufacture*, 65:68-78.
https://doi.org/10.1016/j.ijmachtools.2012.10.006

Chen FJ, Yin SH, Huang H, et al., 2010. Profile error compensation in ultra-precision grinding of aspheric surfaces with on-machine measurement. *International Journal of Machine Tools and Manufacture*, 50(5):480-486.
https://doi.org/10.1016/j.ijmachtools.2010.01.001

Chen HF, Tang JY, Zhou W, 2013. Modeling and predicting of surface roughness for generating grinding gear. *Journal of Materials Processing Technology*, 213(5):717-721.
https://doi.org/10.1016/j.jmatprotec.2012.11.017

Chen HF, Tang JY, Deng ZH, et al., 2018. Modeling and predicting surface topography of the ultrasonic assisted grinding process considering ploughing action. *Journal of Mechanical Engineering*, 54(21):231-240 (in Chinese).
https://doi.org/10.3901/jme.2018.21.231

Darafon A, Warkentin A, Bauer R, 2013. 3D metal removal simulation to determine uncut chip thickness, contact length, and surface finish in grinding. *The International Journal of Advanced Manufacturing Technology*, 66(9-12): 1715-1724.
https://doi.org/10.1007/s00170-012-4452-1

Ding WF, Dai CW, Yu TY, et al., 2017. Grinding performance of textured monolayer CBN wheels: undeformed chip thickness nonuniformity modeling and ground surface topography prediction. *International Journal of Machine Tools and Manufacture*, 122:66-80.
https://doi.org/10.1016/j.ijmachtools.2017.05.006

Ding WF, Cao Y, Zhao B, et al., 2022. Research status and future prospects of ultrasonic vibration-assisted grinding technology and equipment. *Journal of Mechanical Engineering*, 58(9):244-269 (in Chinese).
https://doi.org/10.3901/JME.2022.09.244

Gong YD, Wang B, Wang WS, 2002. The simulation of grinding wheels and ground surface roughness based on virtual reality technology. *Journal of Materials Processing Technology*, 129(1-3):123-126.
https://doi.org/10.1016/S0924-0136(02)00589-7

He YH, Wan RQ, Zhou JJ, et al., 2017. Modeling for surface roughness of hard and brittle materials in axial ultrasonic vibration grinding. *Journal of Vibration and Shock*, 36(23): 194-200 (in Chinese).
https://doi.org/10.13465/j.cnki.jvs.2017.23.029

Hecker RL, Liang SY, 2003. Predictive modeling of surface roughness in grinding. *International Journal of Machine Tools and Manufacture*, 43(8):755-761.
https://doi.org/10.1016/s0890-6955(03)00055-5

Malkin S, Guo CS, 2008. Grinding Technology: Theory and

Applications of Machining with Abrasives, 2nd Edition. Industrial Press, New York, USA, p.115-156.

Setti D, Arrabiyeh PA, Kirsch B, et al., 2020. Analytical and experimental investigations on the mechanisms of surface generation in micro grinding. *International Journal of Machine Tools and Manufacture*, 149:103489. https://doi.org/10.1016/j.ijmachtools.2019.103489

Tao HF, Liu YH, Zhao DW, et al., 2022. Undeformed chip width non-uniformity modeling and surface roughness prediction in wafer self-rotational grinding process. *Tribology International*, 171:107547. https://doi.org/10.1016/j.triboint.2022.107547

Wang QY, Liang ZQ, Wang XB, et al., 2017. Research on modeling and simulation of surface microtopography in ultrasonic vibration spiral grinding. *Journal of Mechanical Engineering*, 53(19):83-89 (in Chinese). https://doi.org/10.3901/jme.2017.19.083

Wang QY, Liang ZQ, Wang XB, et al., 2020. Modelling and analysis of generation mechanism of micro-surface topography during elliptical ultrasonic assisted grinding. *Journal of Materials Processing Technology*, 279:116585. https://doi.org/10.1016/j.jmatprotec.2019.116585

Yang ZC, Zhu LD, Zhang GX, et al., 2020. Review of ultrasonic vibration-assisted machining in advanced materials. *International Journal of Machine Tools and Manufacture*, 156: 103594. https://doi.org/10.1016/j.ijmachtools.2020.103594

Zhang K, Yin Z, Dai CW, et al., 2022. Undeformed chip thickness characteristics in grain-workpiece contact zone in ultrasonic vibration assisted grinding. *Diamond & Abrasives Engineering*, 42(1):88-96 (in Chinese). https://doi.org/10.13394/j.cnki.jgszz.2021.0109

Zhang XF, Yang L, Wang Y, et al., 2020. Mechanism study on ultrasonic vibration assisted face grinding of hard and brittle materials. *Journal of Manufacturing Processes*, 50: 520-527. https://doi.org/10.1016/j.jmapro.2020.01.003

Zhang YZ, Fang CF, Huang GQ, et al., 2018. Modeling and simulation of the distribution of undeformed chip thicknesses in surface grinding. *International Journal of Machine Tools and Manufacture*, 127:14-27. https://doi.org/10.1016/j.ijmachtools.2018.01.002

Zhou WH, Tang JY, Chen HF, et al., 2018. A comprehensive investigation of plowing and grain-workpiece micro interactions on 3D ground surface topography. *International Journal of Mechanical Sciences*, 144:639-653. https://doi.org/10.1016/j.ijmecsci.2018.06.024

Zhou WH, Tang JY, Chen HF, et al., 2019. A comprehensive investigation of surface generation and material removal characteristics in ultrasonic vibration assisted grinding. *International Journal of Mechanical Sciences*, 156:14-30. https://doi.org/10.1016/j.ijmecsci.2019.03.026

Zhou X, Xi F, 2002. Modeling and predicting surface roughness of the grinding process. *International Journal of Machine Tools and Manufacture*, 42(8):969-977. https://doi.org /10.1016/S0890-6955(02)00011-1